Surface circulation in the Gulf of Cadiz: 2. Inflow-outflow coupling and the Gulf of Cadiz slope current

Alvaro Peliz, Patrick Marchesiello, A. Miguel P. Santos, Jesus Dubert, Ana Teles-Machado, Martinho Marta-Almeida, Bernard Le Cann

Surface circulation in the Gulf of Cadiz: 2. Inflow-outflow coupling and the Gulf of Cadiz slope current

Alvaro Peliz,[1] Patrick Marchesiello,[2] A. Miguel P. Santos,[3] Jesus Dubert,[4] Ana Teles-Machado,[4] Martinho Marta-Almeida,[4] and Bernard Le Cann[5]

Received 14 February 2008; revised 3 November 2008; accepted 8 January 2009; published 17 March 2009.

[1] A study of the upper slope circulation in the Gulf of Cadiz is presented. Observations, both original and revisited, and realistic numerical modeling are used together to describe the structure and variability of the slope current system above the Mediterranean outflow. It is shown that the Mediterranean inflow-outflow coupling plays a stronger role than that of the atmospheric forcing in driving the upper slope currents. The Mediteranean outflow forces a surface open ocean current toward the Strait of Gibraltar. Part of it is entrained into the outflow and the remaining flows into the Mediterranean. This latter component does not suffice for the observed transport of the Atlantic inflow into the Mediterranean. A secondary contribution to the inflow is therefore needed to complement the transport. This contribution comes from a persistent equatorward current along the upper slope between Cape St. Vincent and the Strait of Gibraltar. The jet is 20–30 km wide and significant in the upper 200 m attaining subinertial maxima as much as 0.3–0.4 m/s and monthly means in the order of 0.1–0.15 m/s. This current shows a strong variability at time scales in the order of 2–8 days, and displays a significant vertical shear. The response of the upper slope current to synoptic and seasonal atmospheric variability is analyzed. Very low correlation was detected at synoptic scales and the response of the system to seasonal forcing is unclear. A cycle of intensification in June–July and a decrease in winter is apparent in the measurements, but is weak in the model results. It is speculated that the cycle in the observed currents is associated with variability in the inflow/outflow coupling system, rather than driven by seasonally changing wind forcing.

Citation: Peliz, A., P. Marchesiello, A. M. P. Santos, J. Dubert, A. Teles-Machado, M. Marta-Almeida, and B. Le Cann (2009), Surface circulation in the Gulf of Cadiz: 2. Inflow-outflow coupling and the Gulf of Cadiz slope current, *J. Geophys. Res.*, *114*, C03011, doi:10.1029/2008JC004771.

1. Introduction

[2] Despite the growing number of experimental and numerical studies addressing the dynamics of the Mediterranean outflow (MO) [e.g., *Baringer and Price*, 1997a, 1997b; *Jungclaus and Mellor*, 2000; *Serra and Ambar*, 2002; *Borenäs et al.*, 2002; *Papadakis et al.*, 2003; *Serra et al.*, 2005; *Xu et al.*, 2007], the circulation above the MO along the upper slope of the Gulf of Cadiz (hereafter GoC; Figure 1), and the origin of the Atlantic inflow into the Mediterranean Sea have attracted much less attention.

[3] Both *in situ* and satellite observations seem to indicate continuity of the upper slope circulation between west and south coasts of the Iberian Peninsula [e.g., *Folkard et al.*, 1997; *Peliz and Fiúza*, 1999; *Relvas and Barton*, 2002; *Sánchez et al.*, 2006; *Teles-Machado et al.*, 2007]. In particular, SST images show long and cold filaments contouring Cape St. Vincent and penetrating eastward into the warmer GoC waters that suggest a link between GoC upper slope currents and the upwelling dynamics on the west coast (See *Garcia-Lafuente and Ruiz* [2007] for a review.) *Garcia-Lafuente et al.* [2006] and *Criado-Aldeanueva et al.* [2006] reported a series of three dimensional ADCP surveys and concluded that the GoC upper slope is dominated by a persistent surface intensified jet circulating anticyclonically between Cape St. Vincent and the Strait of Gibraltar. However, the dynamics of this Gulf of Cadiz slope current (GCC), and its connection with the inflow and outflow processes and with the Strait of Gibraltar exchange remained obscure.

[4] *Peliz et al.* [2007] (hereafter Part I) showed that the GCC is directly forced by the exchanges at the Strait and proposed a circulation scheme for the GoC as summarized

[1]Instituto de Oceanografia, Universidade de Lisboa, Lisbon, Portugal.
[2]Institut de Recherche pour le Développement, Noumea, New Caledonia.
[3]Instituto Nacional de Recursos Biologicos, IPIMAR, Lisbon, Portugal.
[4]Centro de Estudos do Ambiente e do Mar, Departmento de Física, Universidade de Aveiro, Aveiro, Portugal.
[5]Laboratoire de Physique des Océans, CNRS, Brest, France.

0148-0227/09/2008JC004771

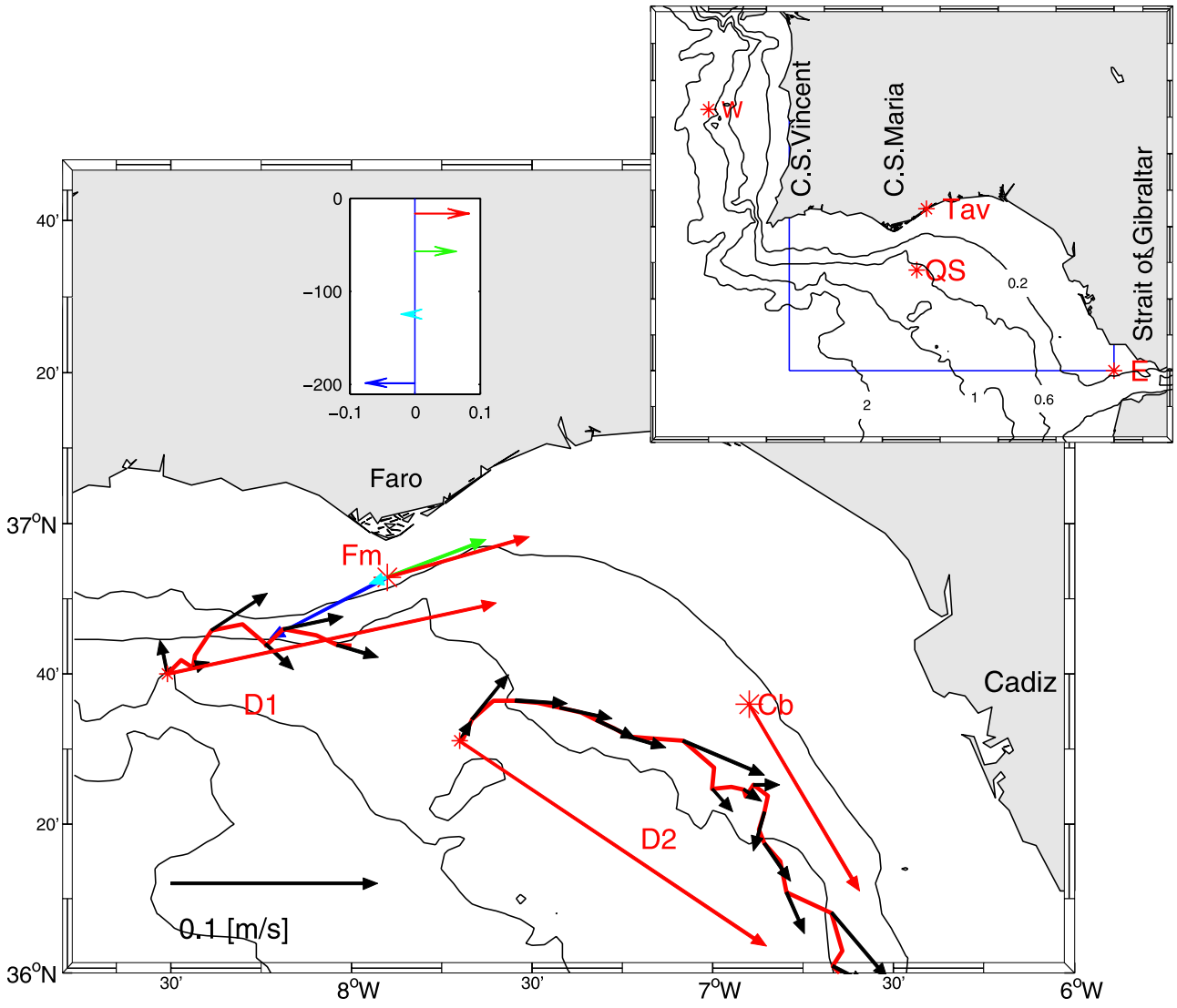

Figure 1. Map of the Gulf of Cadiz slope zone and sites of observations. Vectors represent averaged currents from all the time series. Fm is the Faro mooring (February–June 2006) vectors for the different levels (see left inset). Cb is the residual ($U - U_{ekman}$) subinertial currents from Cadiz permanent recording buoy (1991–2003 with interruptions). Red lines and small black arrows (on a different scale [U * 10]) represent the surface drifter tracks of two SVP buoys (D1 and D2; details in the text). The averaged velocity vector for the represented track is shown in red. Inset shows a map of the southwest of the Iberian Peninsula showing the topography (0.2, 0.6, 1, and 2 km isobaths) and in red the sites of wind time series. Tav, Tavira meteo station; QS, nearest QuikScat grid point to Tav; W, west point representative of west coast conditions; E, east point off the Strait of Gibraltar.

in Figure 2. The interaction of the Mediterranean Outflow with topography and the entrainment process induce significant circulation in the surface layer. This circulation is constituted of an Offshore Inflow current that feeds the MO cores and part of the Atlantic inflow. Inshore, a second current is generated to complement the necessary transport for the inflow (inshore inflow or GCC). The Atlantic inflow therefore is a sum of these two components. Nevertheless, Part I addressed only the mean flow structure. Here we (1) compare model results with observations and (2) analyze the influence of seasonal and synoptic atmospheric forcing on the GCC.

[5] The data and methods are described in section 2. Since the model is described in Part I, only a short description of the modified aspects is provided in section 3. Section 4 is dedicated to the analysis of inflow-outflow coupling in the observations and in the model. Section 5 describes the GCC variability at synoptic and seasonal scales from observed data. In section 6, model time series are analyzed. Finally, in section 7 we present the discussion and conclusions.

2. Data

[6] In this paper, we use revisited and original current-meter and wind data of different sources. Some of the data are published in other papers, and the reader is referred to the respective references along the text for details. For synoptic and seasonal variability analysis, we use two sets

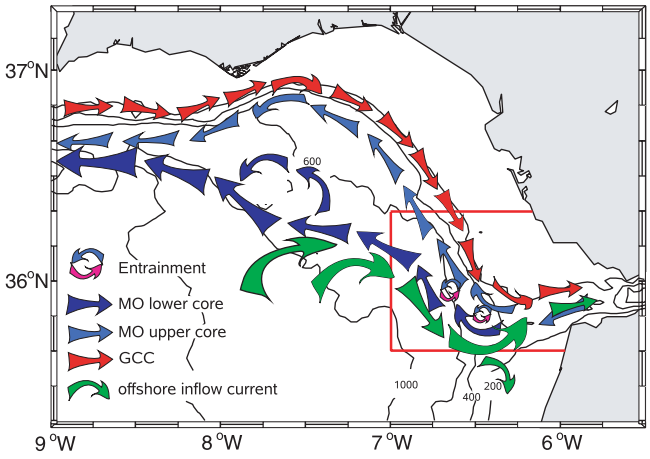

Figure 2. Schematic representation of the mean Gulf of Cadiz slope current system. The blue arrows represents the Mediterranean outflow upper and lower cores. Bright red arrows represent the mean path of the inshore inflow (the Gulf of Cadiz slope current (GCC)), and green arrows stand for the offshore inflow. Red box indicates the sections for the GCC transport balance calculations (presented in Figure 15).

of wind and currentmeter data from two different periods. A longer period used mainly for seasonal analysis, is based on the time series of Cadiz buoy (Cb) winds and currents. To analyze the synoptic variability we use original data from a mooring south of the St. Maria Cape (which is next to Faro) together with wind time series of the same period but from different sites of the GoC. For convenience we will refer to this second set of currents and wind data as Faro mooring (Fm). Figure 1 shows the location of the observation points.

2.1. Currents

[7] The data set from Cb is fully documented and available upon request from Puertos del Estado (www.puertos.es) Oceanography and Meteorology division. Both winds and currents are provided on hourly values and at 3 m high and 3 m depth respectively.

[8] Currentmeter records near Faro (Fm; Figure 1) were obtained between 1 February and 10 June 2006 by the Portuguese Fisheries and Sea Research Institute (IPIMAR) from a mooring deployment off the St. Maria Cape. The mooring consisted of 4 Aanderaa Rcm 9 acoustic sensors programmed for an acquisition at 5 min intervals. The instruments were deployed at nominal depths of 10, 50, 120, and 195 m approximately over the 205 m isobath.

2.2. Winds

[9] Figure 1 (inset) indicates the different sites for which wind vector time series were measured or simulated using the atmospheric model (described below). Winds at Cb for the period 1999–2003 were made available by Puertos del Estado.

[10] For the Fm period, we use coastal winds measured at Tavira automated weather station (Tav; inset of Figure 1) obtained from Instituto Hidrografico (Portugal). Offshore winds for a point near Cape St. Maria (QS; inset of Figure 1) were extracted from QuikScat surface reanalysis of CERSAT (Ifremer, France). Winds for 2006 were extracted from Weather Research and Forecast (WRF V2.0) model simulations in the observation sites (QS, Tav), as well as in two additional points; one west of Iberian Peninsula (W; inset of Figure 1), and the other in the eastern part of GoC, right off the Strait of Gibraltar (point E).

2.3. Drifters

[11] Despite the growing amount of worldwide surface drifting buoy data, the GoC is poorly sampled. Only two surface buoys drogued at 15 m (28692 in March–April 2003 and 15074 in April 2001) were present in the Surface Velocity Programme (SVP; www.aoml.noaa.gov/envids/gld) database. These float tracks are represented in (Figure 1, red lines). The red arrows represent the mean current for the period shown, and the black ones (at a different scale) show daily mean values.

[12] A subsurface RAFOS type float is also used. It corresponds to two 90 day underwater cycles of a multicycle float (Marvor 407, cycles 07 (13 March to 10 June 1998) and 08 (13 June to 10 September 1998)) from the French project ARCANE [*Bower et al.*, 2002]. This float was drifting at a nominal pressure of 450 dbars and was tracked using a sound source array from several US and European partners. Between the two cycles, the float surfaced for ~2 days in order to transmit data, and float tracking proved difficult for the last 30 days of cycle 07.

3. Model Configurations

[13] A full description of the model and experiment configurations is given in Part I and will not be repeated here. Contrary to Part I, here we use realistic atmospheric fields. Two main numerical modeling experiments are analyzed in the scope of the present paper: A short-period experiment with simulated atmospheric fields for the first semester of 2006 covering the period of the Faro mooring (hereinafter Exp1), and a longer run for the years 2001–2002 (Exp2; partially covering the Cb mooring data) with atmospheric forcing from global databases. The initial ocean state, lateral forcing and the Gibraltar Strait boundary condition are the same as for Part I. Also, a better representation of the model MO properties was obtained by adding a Smagorinsky scheme for tracer diffusion in the simulations of the present study.

[14] For the period 2001–2002, and to analyze seasonal variations, we use NCEP air-sea fluxes reanalysis (www.ncep.noaa.gov) and QuikScat reanalyzed winds from CERSAT (cersat.ifremer.fr). For the period 2006 (coincident with Fm mooring), and to analyze the response of the upper slope flow to synoptic forcing we simulated the atmospheric forcing with WRF. The atmospheric grid was 15 km resolution with 46 vertical levels. Nonhydrostatic mode, third-order Runge-Kutta time integration and fifth/third-order spatial discretizations for horizontal/vertical advection terms were used. For diffusion we used a Smagorinsky scheme, and Mellor-Yamada-Janjic TKE for the planetary boundary layer. The model was initialized by interpolating NCEP fields to the model grid. Lateral and sea surface conditions were interpolated from 6-hourly NCEP fields and from SST with weekly Reynolds SST values, respectively. Figure 3 shows the time series of surface winds from observations (Figures 3a and 3c) and from WRF simulations

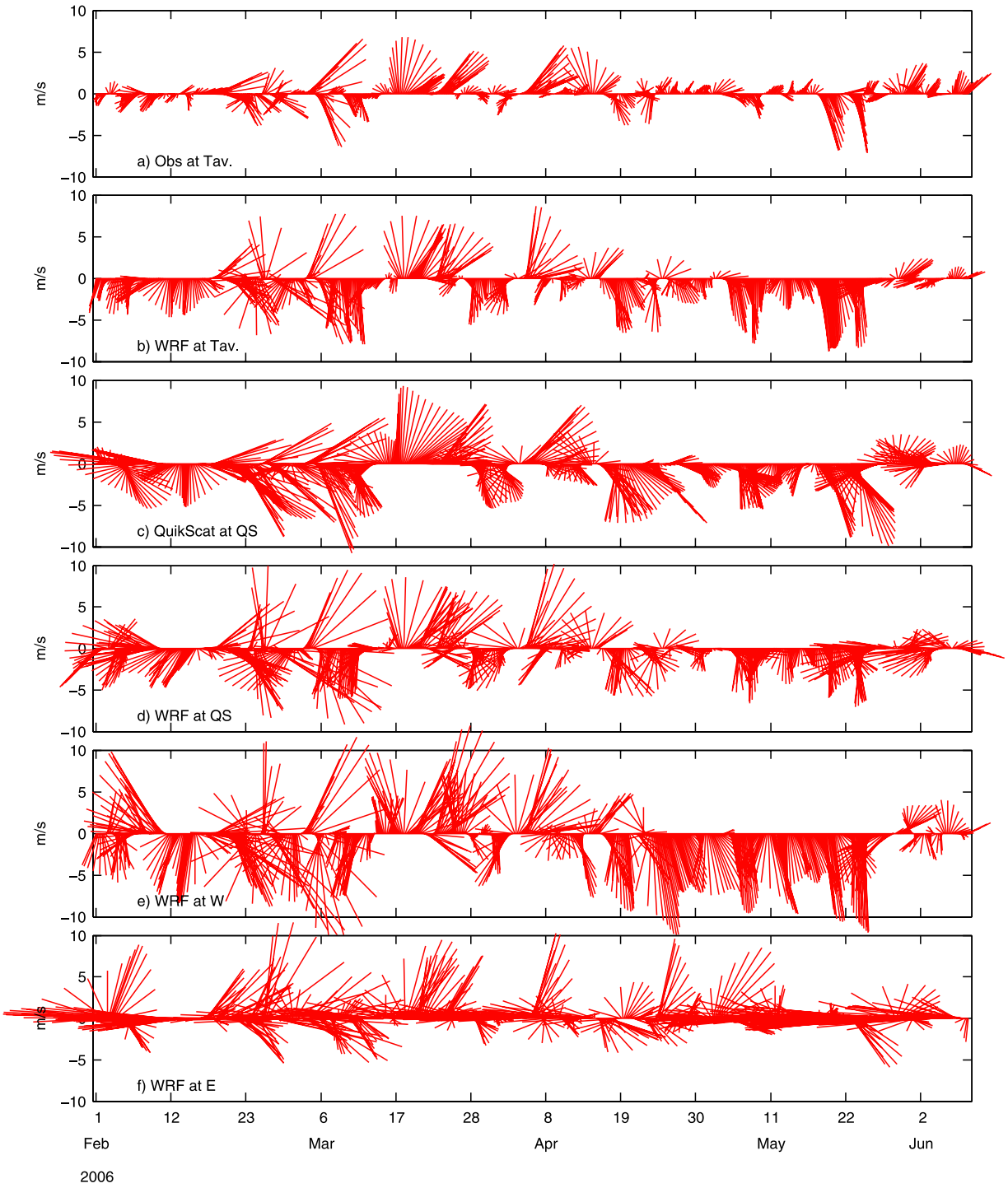

Figure 3. Measured and model wind vector time series for the different sites indicated in the Figure 1 inset for the period of Fm experiment (in 2006). All winds were filtered to evidence subinertial variability.

(Figures 3b, 3d, 3e, and 3f). The simulations cover the period from January to June 2006, but the plot represents the period of Fm data only.

[15] In the upper four stick plots, we observe a good match between simulated and observed winds. Figure 3a shows the wind vectors at Tavira coastal station (Tav), and Figure 3b shows WRF winds interpolated to the Tavira meteo station position. The model winds follow the observed ones well, in general, but are stronger (Kundu vector correlation 0.8 [*Kundu*, 1976]). The model overestimation may be due to drag effects over land not properly accounted for, or to a poor representation of prominent orography features north of Tavira station. We used the modeled winds at different locations (Figures 3d–3f from the sites QS, W, and E; Figure 1) for comparison with the currentmeter time

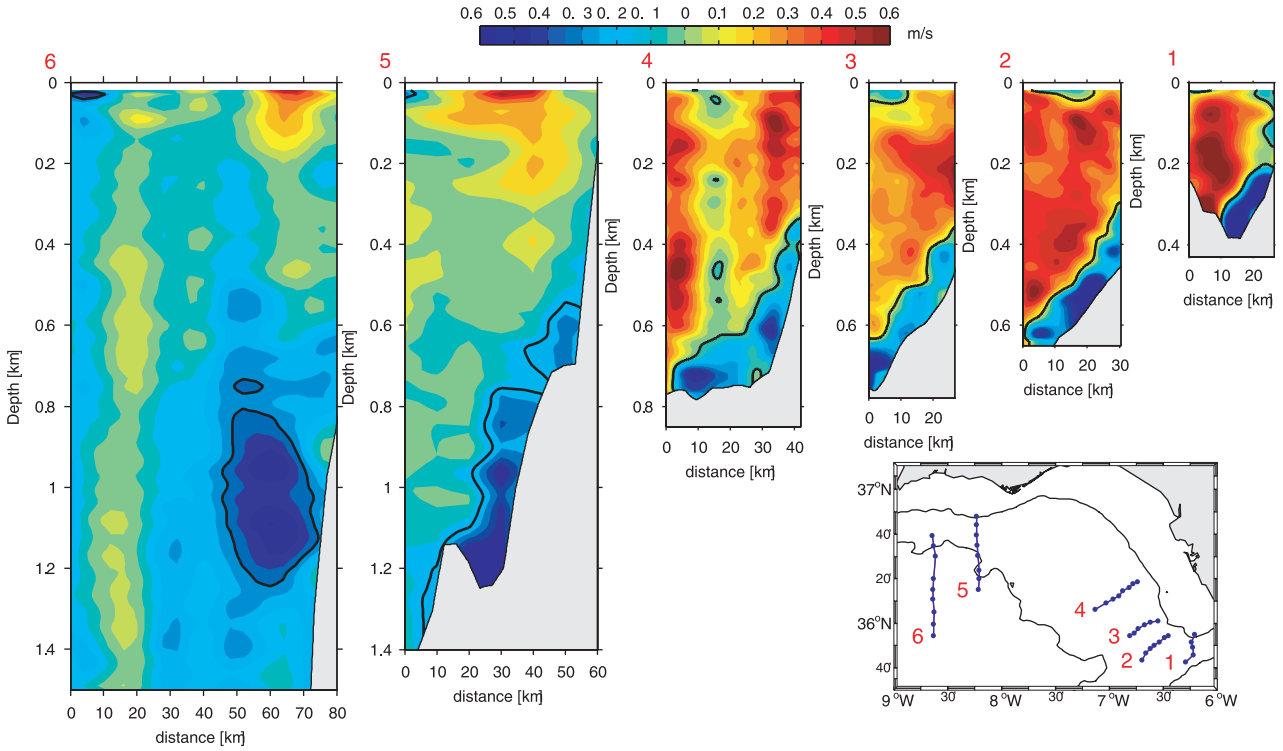

Figure 4. Alongshore (cross-section) flow at different sites on the basis of XCP sections of *Baringer and Price* [1997a]. Positive means alongshore equatorward (the Mediterranean outflow is negative). The bottom right inset shows the locations of the different sections (1–6) numbered from the strait westward.

series, and to analyze wind-current covariance in the Fm period.

4. Inflow/Outflow Coupling in the Observations and in the Model

[16] We concentrate on the coupling between the Mediterranean Outflow cores and the upper layer flow. For clarity, the term "core" (lower/upper core) is used when referring to the Mediterranean Outflow, and Offshore/Inshore inflow current when the discussion focuses on the flow above the MO (see Figure 2).

[17] A focal point of the entire slope current system is centered in a small area near 6.5° W, 36° N. In this area, the outflow starts its strong interaction with the sloping bottom, increasing velocity and mixing with ambient water. Data from a synoptic survey of this area in fall 1988 with Expendable Current Profilers (XCP) [*Baringer and Price*, 1997a] is revisited here. Figure 4 shows the cross-section velocity (with positive values alongshore-equatorward), and Figure 5 displays the vector fields of the depth integrated layers: the layer above the MO and below the 50 m depth (Figure 5a), the MO defined as the layer between the bottom and the zero-crossing interface (for the cross-section velocity)(Figure 5b), and an intermediate layer between 380–450 m (Figure 5c). Finding a velocity reference with XCP's was difficult and we concentrated on the flow structure rather than on velocity values.

[18] The MO in Figure 4 (negative values), and in Figure 5b shows evidence of double core flow that could be an early sign of splitting. The upper layer also evidences a double core flow (the confluent Offshore and Inshore flows) especially at section 4 (Figure 4). In Figure 5a, the inflow is partially fed by an offshore inflow contouring the MO outer edge (lower core), and a coastal current above the upper core.

[19] Across-slope model sections for different parts of the GoC are presented in Figure 6. The values correspond to cross-section velocities of monthly averages for June and December taken from the 2-year simulation of Exp2 (Note that the model sections are not in the same scale as the XCP sections of Figure 4. However, this representation was preferred in order to show the whole structure of the slope flow). The model MO structure is very similar to the XCP observations with the cores being at the same depths, and velocity values of the same order. The depth intensification of the Offshore Inflow current (or MO counterflow) above the MO deeper edge is noticeable in sections 1–3. Although some variability in flow intensity and position is observable between different time outputs, the double jet structure of the upper flow is fairly constant between the different seasons (Figure 6).

[20] Further information on the generation of the Offshore Inflow current is reported in Figure 7. Figure 7 represents a RAFOS float data at ~450 m depth, that entered the Gulf of Cadiz and was captured in the inflow/outflow coupling zone. The track is represented in red when the float traveled into the slope zone, and in blue after being trapped along with the slope current system. The float entered the slope region from the southwest, and near 7° W it was captured by the Offshore Inflow and drifted southward with velocities around 0.1 m/s. Very close to the slope, the float described a series of concentric cyclonic loops while it was retained for about a month. These loops are slightly elliptic, with maximum major axis ~15 km, aligned alongslope, and

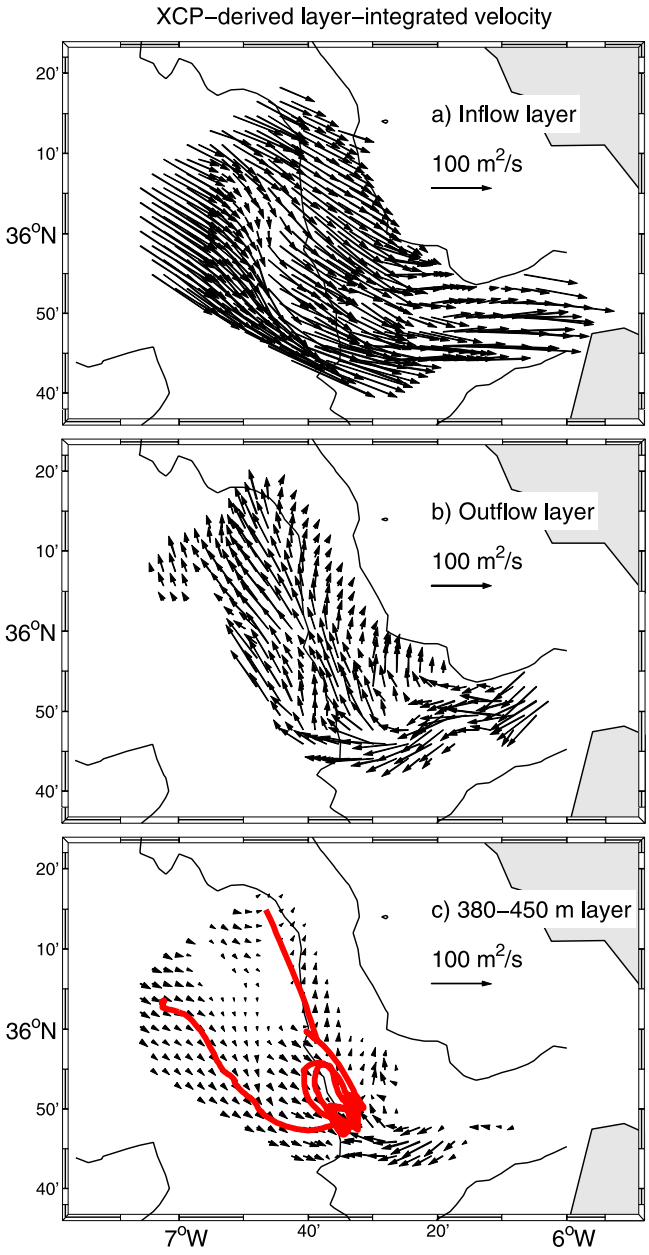

Figure 5. Vertically integrated velocity vectors for (a) upper layer (from 50 m depth to the flow inversion), (b) outflow layer (from the inversion to the bottom), and (c) intermediate 380–450 m layer. Values below 15 m^2/s were not considered. The red lines show the track of the RAFOS float that drifted into the zone.

maximum minor axis ~10 km. Afterward the float was caught inside the Mediterranean Outflow upper core and progressed westward along the slope. During its slope trip (blue part of the track), the float started to drift at depths of about 380 m and deepened in the westward direction. With the exception of two small meanders before 7° W the float speed was fairly regular and around 0.3 m/s. Around 8.30° W near Portimao Canyon, the float seems to have been ejected from the slope region at depths about 460 m and lost its speed to values close to 0.1 m/s.

[21] The portion of the float track that was near the slope off the Gibraltar Strait is represented in Figure 5c. Black arrows are XCP values integrated for the depth layer range 380–450 m where the float was drifting. Although the measuring periods are very different and despite all the interpolation and averaging of XCP data, a good match is observed between the float track and the vector field direction, and the cyclonic looping is observed in the region of inflow/outflow coupling and entrainment zone.

[22] The same part of the float track is overlaid on one model output vector field, which is averaged for approximately the same depth layer (~400 m) in Figure 8. It is noticeable that the cyclonic looping of the float and the standing cyclone in the model output are coincident. Moreover, the float track portion that corresponds to upper core MO is very similar to the flow described by the vectors. The main difference between the float track and the flow described by the vectors, corresponds to the outer part of the Offshore Inflow current. The vectors seem to describe a sharper southward turn and the bulk of the flow seems to be inshore of the float track. In the case of the XCP observations (Figure 5), the flow appears to be offshore of the float track. However, these small differences are averaged out if different model outputs are considered. It is noticeable from the monthly averages presented in Figure 6 that the flow structure is rather constant along its path.

[23] The float track describes the very same flow path recurrent in the model results and in the mean circulation fields calculated in Part I (see flow field and stream lines of Figures 11–14 of Part I), providing further confirmation of the flow structure near the inflow/outflow coupling zone depicted in the scheme of Figure 2: An offshore flow is forced slopeward along the outer edge of the MO; depending on the depth level, part of this slopeward current is entrained either within the MO lower core for depths below about 600 m, or within the MO upper core (like the case described by the float in Figure 8); at shallower levels, it either merges with the Inshore Inflow current to feed the Atlantic inflow or it recirculates southward; in this inflow/outflow coupling zone, the current curls cyclonically generating a standing eddy, in which the drifting float was trapped. This standing eddy is reproduced in the model outputs. The Offshore Inflow part that reaches the Strait does not complement the necessary transport toward the Mediterranean Sea; a second coastal Inflow current (the GCC) is therefore needed to close the mass balance.

[24] In sections 4–6 of Figure 4, the GCC is a surface intensified jet of about 20–30 km wide with depths of around 200–300 m, and with speeds in the order of 0.2–0.3 m/s. Approximately the same values are reported in *Garcia-Lafuente et al.* [2006]. These flow scales match those of the model in the sections of Figure 6. However, in most of the model situations, the current shows a considerable degree of topographic control in the western part of the domain (section 6 in Figure 6), and rarely detaches from the upper slope, as is apparent in sections 5 and 6 of Figure 4. *Garcia-Lafuente et al.* [2006] also reported this. The remaining of the paper will be dedicated to the time variability of this flow feature.

5. GCC Variability

[25] Figure 1 presents a summary of the different current measurements gathered for this study. The map shows mean

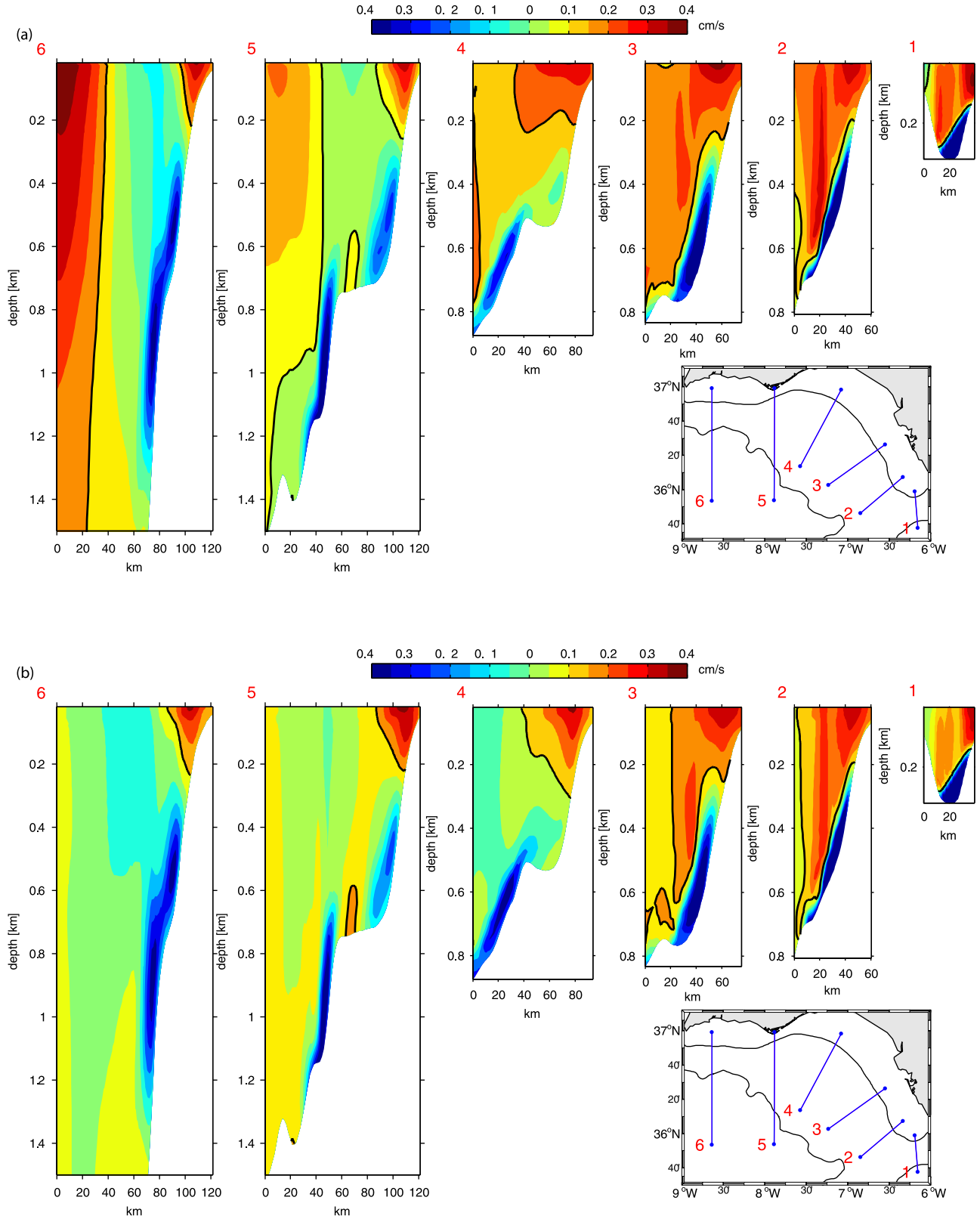

Figure 6. Model cross-section velocities averaged for (a) June and (b) December using data from experiment Exp2. The sections are represented in the bottom right insets. Positive velocities indicate equatorward flow (the MO is negative).

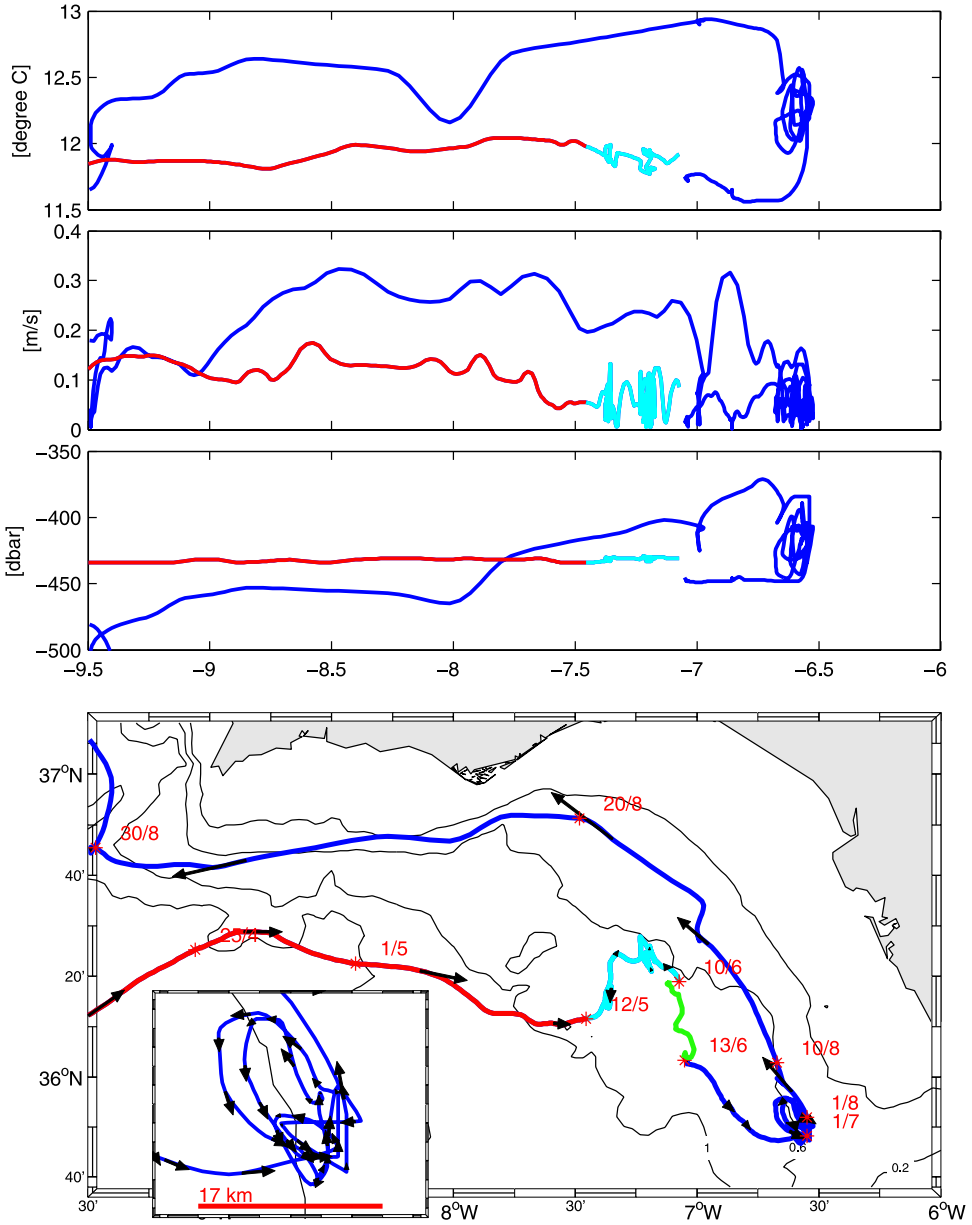

Figure 7. Multicycle RAFOS float (Marvor 407) at nominal pressure 450 dbars that entered the Gulf of Cadiz in spring 1998. (top) Temperature (°C) as a function of longitude; (top middle) float speed (m/s) as a function of longitude; (bottom middle) float pressure (dbars) as a function of longitude; (bottom) float track. Two underwater cycles are plotted (in red for cycle 07 and blue for cycle 08). On Figure 7 (bottom), these two cycles are separated by ∼2 days surface track in green. Because of tracking difficulties, underwater positioning was more noisy during the last 30 days of cycle 07 (in light blue). The 2, 1, 0.6, and 0.2 km isobaths are represented. The inset zooms the track over the inflow-outflow coupling zone to highlight the cyclonic looping. The 0.6 km isobath is plotted in black, and a scale is indicated (in red).

vectors for the Faro Mooring (Fm in February–June 2006, in detail in Figure 9), the mean for the long period off Cadiz permanent recording buoy with current measurements at 3 m (Cb in 1999–2003 with interruptions; time series shown in Figure 10), and two drifting buoys (D1 and D2) of the Surface Velocity Programme (drogued at 15 m). In the case of Faro mooring, the currents were measured at different depths and the mean vectors are also represented vertically disposed in the inset of Figure 1. The different sources of data show a clear tendency for a surface along-slope equatorward current with mean averaged speed in the order of 0.1 m/s, although the subinertial maxima may be as high as 0.4 m/s. Despite the differences in the recording periods and measurements, an intensification of the slope current in the eastern part of the slope (east of Cape St. Maria) is apparent. Both drifting buoys enter the slope zone from

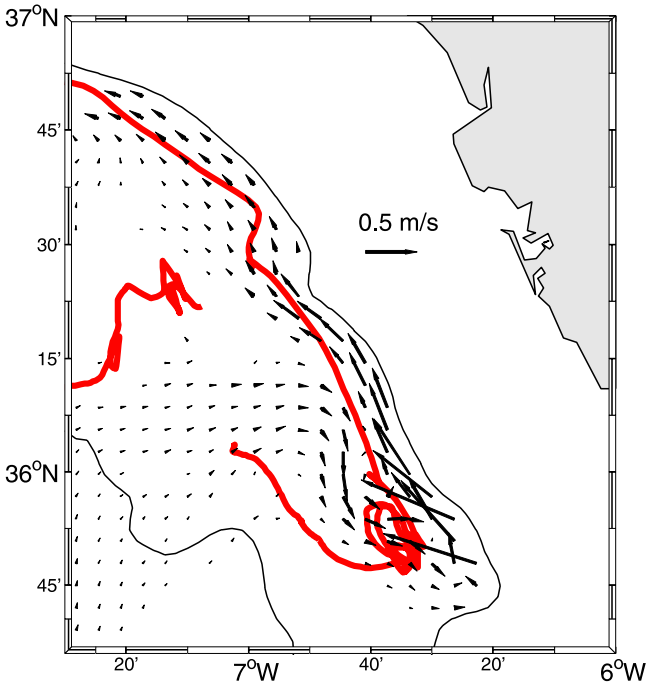

Figure 8. Model velocity vectors at 400 m depth (average of 1 month of simulation during Fm 2006 experiment) in the zone of inflow-outflow coupling. The RAFOS float track is overlaid in red.

offshore and speed up equatorward with velocities in the order of 0.2–0.25 m/s.

5.1. Cb Data and Seasonal Variability

[26] The long-term series of residual subinertial currents of the Cadiz buoy (Cb) is presented in Figure 10. The series is incomplete as only periods of overlapping wind and current data were considered. The series were filtered to obtain only subinertial variability, then the Ekman contribution was removed from the currents. Winds show a northwesterly predominance, but a significant variability with reversals to southerlies or southeasterlies is common to the entire wind vector time series. The dominant current direction is southeastward and coincident with the slope orientation. Very few clear reversals are observed in the current time series and they occur mostly in the winter season. An intensification in summer months is also apparent.

[27] Monthly mean wind vectors (black) and currents (blue) calculated using the entire period of the Cb are represented in Figure 11. The lines show the currents along-isobath component monthly mean (solid) and subinertial maxima (dashed-dotted line). The same representation is used for the shorter Fm mooring (green) and for the model results of experiment Exp2 (red). Although the drifting buoy records are rather short (of the order of only several days) they are also represented together with the monthly current averages because they give us a scale of instantaneous values.

[28] With the exception of December, the monthly averaged currents are equatorward almost year-round, yet a seasonal intensification in summer and a decrease from November to January is observed. The mean monthly vector time series for winds (black) and currents (blue) do not show a clear covariance pattern during all months. The variability of the mean wind direction is much larger than that of the current. For the months of March and October there is a reversal of mean wind direction not followed by changes of any great significance in the mean current (although a weakening is clear). For the winter months (November–January), the mean current consistently slows down, but the mean wind values vary significantly from one month to the other. On the other hand, a small change in winds from January to February corresponds to a significant difference in mean currents, and the same can be said for the period between October and December. The monthly subinertial maxima do not show any clear seasonality but for a small, but noticeable tendency toward higher values in summer. The Fm monthly means (analyzed below) show good agreement with the Cb values for mean and maxima. A feeble decrease in March is also noticed which may be coincidental (since the observation period is different at Fm and Cb), although the same signal is reproduced by the model as will be discussed later.

[29] An analysis of the Cb wind residual current covariance was conducted by using Kundu vector correlation [*Kundu*, 1976]. Direct correlation between both series yielded very low correlation coefficients. We have filtered the series with a 6-day window and then recalculated the vector correlations that increased almost to 0.4, but only at the zero time lag (see Figure 12a). To understand how the winds residual current covariance varies along the year, we calculated the zero lagged vector correlations for subseries of 20 days in a running box fashion, and obtained a series of correlations coefficients. Monthly averages of these series were calculated and are represented in Figure 12b. It is clear that correlations increase for late spring-early summer months (peaking in June) with very weak values for the remaining period as could be expected from the analysis of the monthly averages provided before.

5.2. Fm Data and Synoptic Variability

[30] Figure 9 shows the Faro mooring subinertial current vector time series at different depths. It can be observed that the current direction has more variability and frequent reversals than at the Cadiz buoy (Figure 10). These time series present significant variability in the order of a few days with reversals occurring over periods of 2–8 days. An interesting feature is the vertical shear in the mean currents (see Figure 9 and inset of Figure 1). The currents below 120 m are dominantly westward with intensified events around mid-March. Figure 13 shows the alongshore flow averaged over 15-day periods at different levels (eastward/equatorward flow is positive). The vertical shear is approximately maintained during the sampling period but a significant tendency for westward flow in March is observed. After April, the water column restratifies (see Figure 9a) and interestingly the layer above 120 m seems to respond more barotropically with eastward flow (Figure 13) although at the deepest observed level, the current remains westward. The origin of this westward flow is unclear. We have no salinity data to support a link of this shallow current with water of Mediterranean origin, and the shallowness of this mean westward flow is surprising as neither models nor

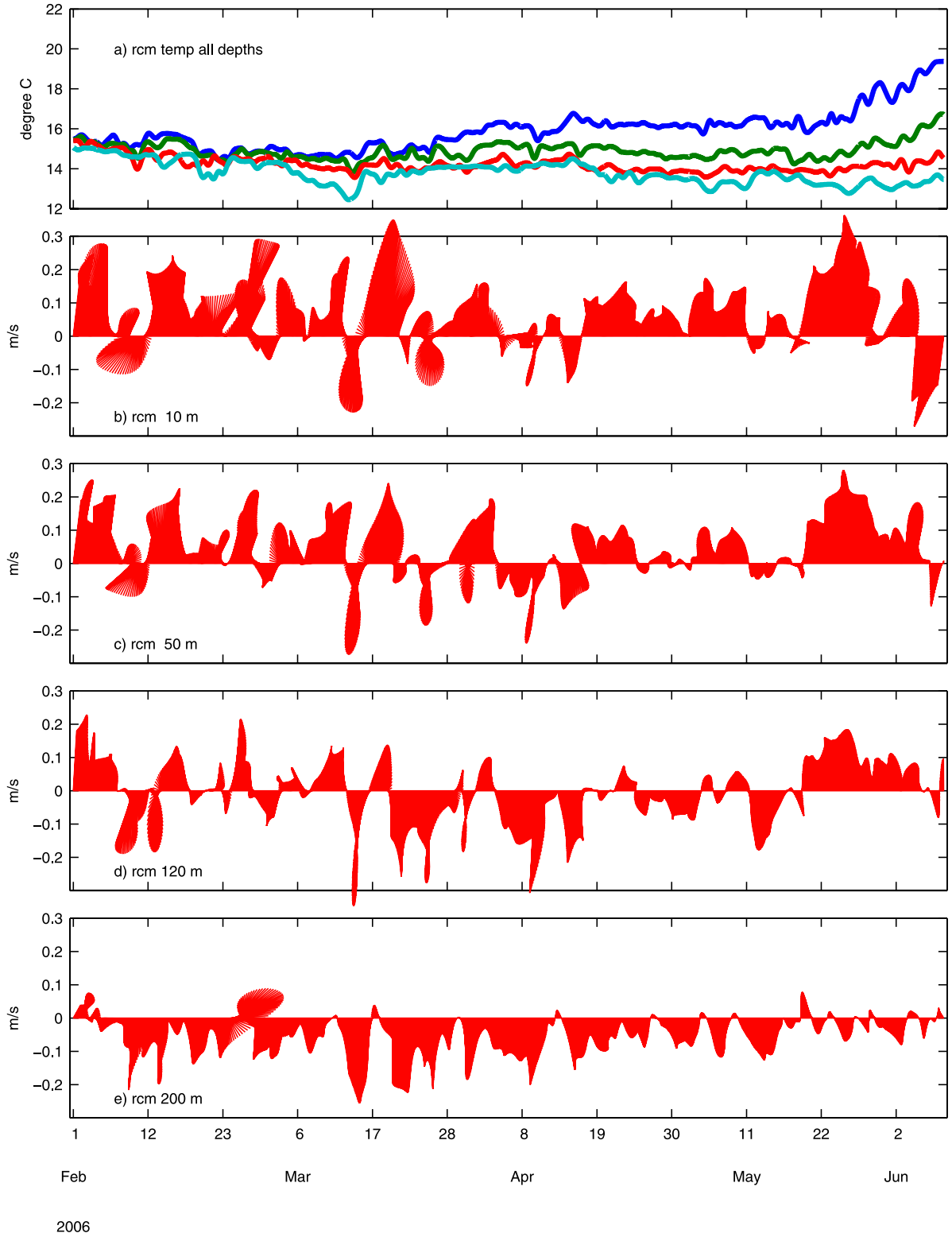

Figure 9. Faro mooring (Fm) subinertial (a) temperature at all depths (10 m in blue, 50 m in green, 120 m in red, and 200 m in light blue) and (b–e) hourly time series of current vectors at different depths. Current values are rotated (70°) such that y axis indicates alongshore direction (positive is eastward/equatorward).

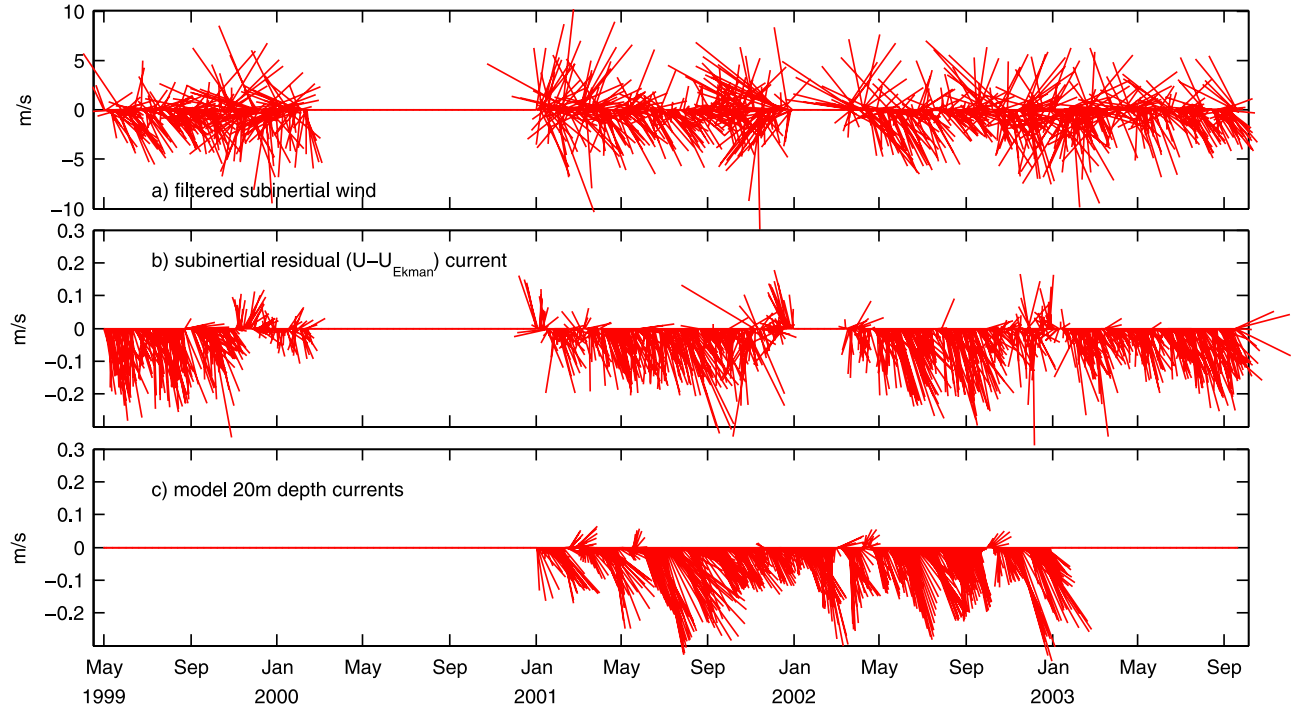

Figure 10. Cadiz buoy (Cb) data (a) filtered winds, (b) residual ($U - U_{ekman}$) subinertial currents, and (c) subinertial model currents (20 m depth) for the Cb zone (model simulations were limited to the 2001–2002 period). In order to obtain residual currents, only periods overlapping good wind and current data were considered.

observations have yet revealed any evidence of a Mediterranean upper core as shallow as the flow described here.

[31] To investigate if this high-frequency variability (2–8 days periods) is associated with local wind forcing at synoptic scales, over the Gulf of Cadiz region, we extracted wind vector times series from several points of the region. The point (QS, Figure 3d) close to Cape St. Maria was selected as being representative of the wind forcing near the currentmeter location. WRF time series was extracted for the West part of the Iberian Peninsula (W; Figure 3e) because it represents the atmospheric forcing along the west coast and is thus indicative of upwelling activity. An additional time series near the Strait of Gibraltar (E; Figure 3f) is representative of the surface forcing of the Atlantic inflow into the Mediterranean.

[32] The wind field evolution (Figure 3) can be divided into three main periods: (1) February to mid-March, winds were variable with dominant northerlies; (2) mid-March to mid-April, winds were variable with dominant southwesterlies; and finally (3) after mid-April the winds were persis-

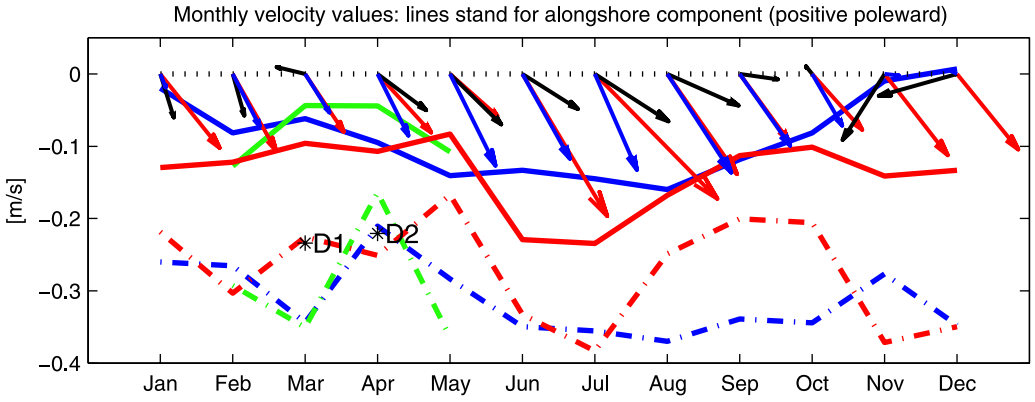

Figure 11. Monthly means of winds [U_{wind}/10] (black vectors). Monthly averaged current vectors for Cadiz buoy (Cb) data (blue vectors) and for the model results at Cb site (red vectors). Monthly averaged alongshore flow (solid line) and monthly maximum (dashed-dotted line) for the Cb data (in blue) and for the model data (in red). Averaged velocities for the drifters D1 and D2. Fm-averaged alongshore flow (green solid line) and monthly maximum (green dashed-dotted line) are also represented.

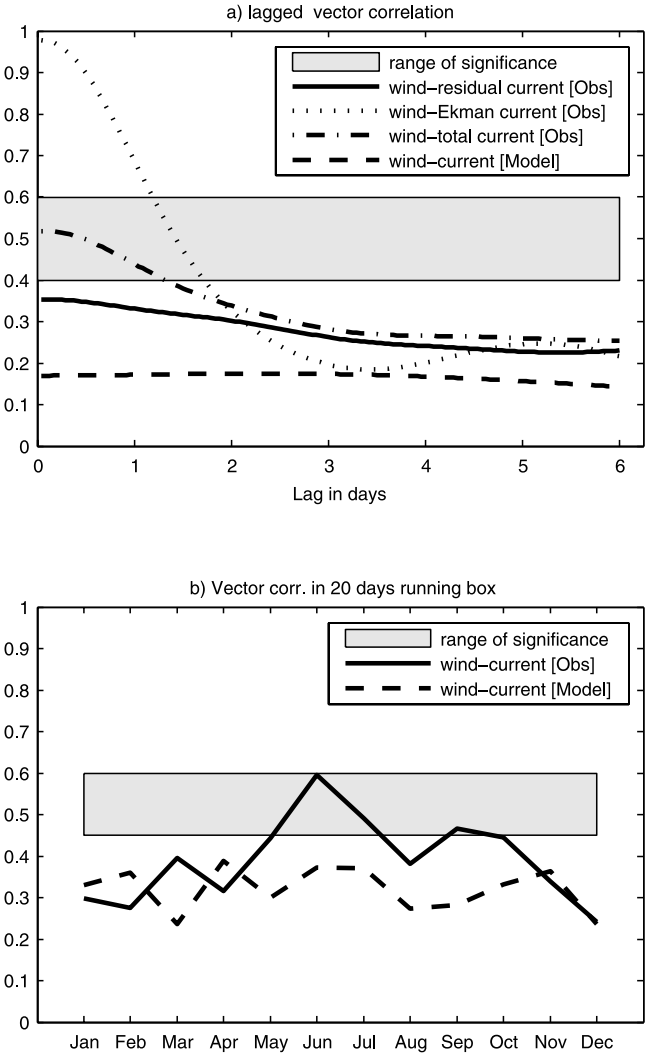

Figure 12. Kundu vector correlation analysis [*Kundu*, 1976] between winds and currents. (a) Lagged wind-currents correlations for Cb time series (Figure 10). (b) Monthly means of 0 lag correlations in periods of 20 days (running box) for the Cb wind residual currents time series (Figure 10). Solid lines stand for the observations, and dashed lines stand for the model data. To decrease short-period oscillations, the series were filtered with a 6-day window. The gray bar denotes a range of significance. The lower bound is calculated with more conservative criteria (lowest estimate of the degrees of freedom and 1% confidence limit). The upper value corresponds to a less restrictive estimate (highest value of the degrees of freedom and 5% confidence limit). The degrees of freedom were calculated on the basis of the structure of the autocorrelation functions for the modulus of the series.

tent from the north with a relaxation after 26th May. The winds at the west and south coasts (W and Qs) were fairly similar during the first two periods, but the south coast winds were much weaker during the later northerlies period. In point E (Figure 3f), the winds were generally zonally oriented because of the influence of the Strait, and rarely agreed with the other time series. Some similar periods can be distinguished in the Fm current time series (Figure 9). The mid-March to mid-April period was characterized by stronger westward flow, particularly below 120 m. Prior to this period, the surface currents were clearly eastward and after mid-April the eastward flow was dominant. However, there are no clear transition between these periods and the change by mid-March was also coincident with the beginning of the restratification (Figures 9 and 13).

[33] The apparent correspondence between the periods may not indicate a linear relation between wind and the Fm currents. A Kundu covariance analysis between winds and currents for Fm time series was conducted. In order to eliminate short-scale variability, the vector time series were filtered for periods less than 6 days. The values indicated even smaller correlations between winds and currents than those obtained using Cb data (generally below 0.3). More complex analysis using wavelet covariance and coherence was used but did not bring a more conclusive pattern. Significant covariance values are obtained for just a few periods but with contradicting results concerning the phase spectra. To summarise, besides the visual comparison (Figures 3, 9, and 10) and the monthly values in Figure 11, the covariance analysis indicates that there is no clear first-order response of the GCC to the local wind forcing nor to wind forcing along the west coast of Iberia or near the Strait of Gibraltar. This fact supports the hypothesis that the GCC is dominated or at least partially forced by the inflow into the Mediterranean and by the adjustment of the outflow and entrainment processes.

6. Model GCC Seasonal and Synoptic Variability

[34] Two model experiments were conducted for the 2001–2002 period, and for the first semester of 2006 in order to compare the model results in Cb and Fm. In the case of the 2001–2002 period, the runs were conducted using QuikScat winds and NCEP heat fluxes to represent the atmospheric forcing conditions. For the case of 2006, WRF simulated winds were used.

6.1. Seasonal Variability

[35] Model 20 m current vectors in the Cadiz buoy zone are represented in Figure 10c. The model represents fairly well the current directions and intensities although some more sharper reversals are noticeable in the model currents

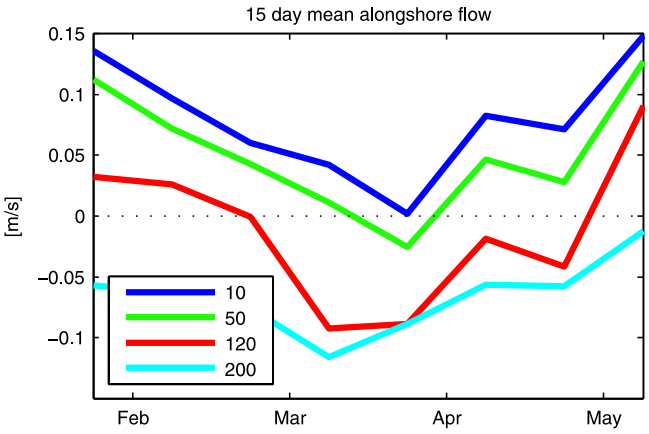

Figure 13. Alongshore 15-day means for the Fm mooring at different depths.

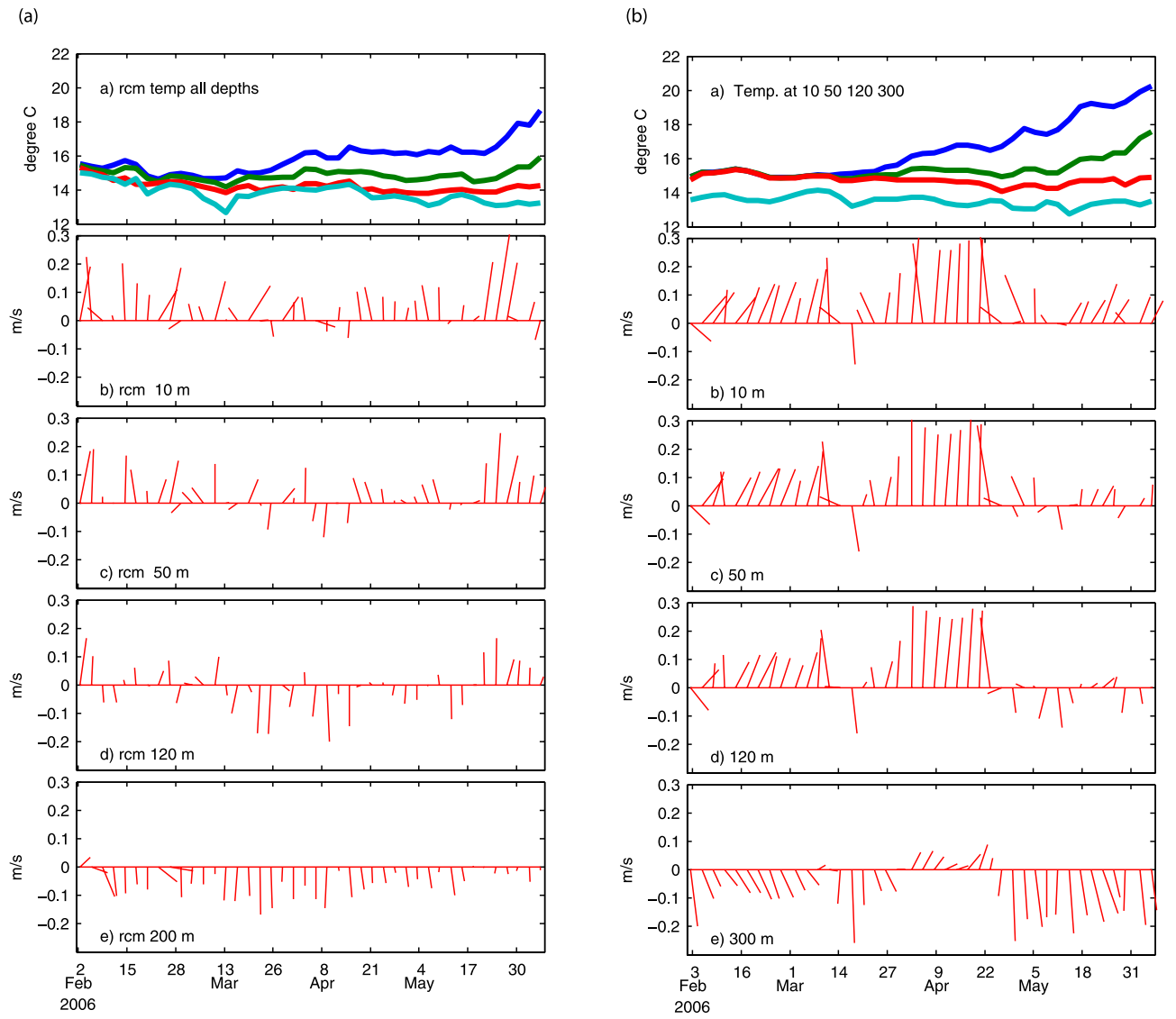

Figure 14. (a) Observations and (b) model 3-day averaged time series for Fm mooring (for the observations Figure 14 reproduces the same as in Figure 9 with averaging). In the case of the model the time series were extracted one grid point to the south to allow an extraction of values at 300 m instead of 200 m in the observations (see text). For the temperature the color coding is as following: 10 m in blue, 50 m in green, 120 m in red, and 200 (300 in the case of the model) m in light blue.

than in the observed ones. The model vector time series seems to be dominated by event-scale variability and no clear summer intensification is seen (like the one that is apparent in the observed currents Figure 10b). The model monthly mean currents (along-shore component) are represented in Figure 11 (red sticks and lines) together with monthly averaged Cb values. It is interesting to notice that model monthly averages follow the observed values reasonably well along the year (even the spring decrease seems to be simulated) but in the winter months of November–January, they diverge (see red and blue solid lines in Figure 11). The model does not represent the GCC slow down during winter months. A wind model current Kundu correlation analysis was conducted using the same method as for the observed currents (sea Figure 12b dashed line). The correlations for the model vector time series are close to the observed ones during spring-winter but much lower during summer, and below the significance level year round.

[36] Assuming that the seasonality in the atmospheric conditions are being well represented in the model, the fact that the GCC does not slow down may be an indication that either the imposed Strait of Gibraltar condition is not correct for these winter months, or that a third external factor not accounted for in the model is playing an important role. We may speculate that a likely candidate is the open ocean influence associated with the large-scale meridional density gradients, which are known to setup a winter intensified upper slope poleward circulation on the northwestern margin of Iberian Peninsula [see *Huthnance*, 1984; *Frouin et al.*, 1990; *Peliz et al.*, 2003a, 2003b, 2005]. The same mechanism, although to a different degree, may play a role in the GoC slope currents as well.

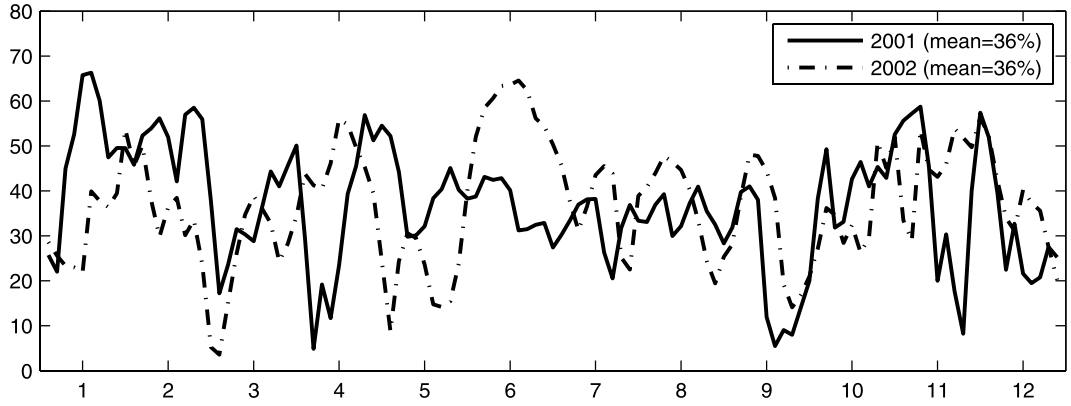

Figure 15. Time series of the estimated contribution of the GCC to the inflow based on the percentage of transport across the northern part of a box to the west side of the strait (red box in Figure 2). The solid line stands for the 2001 experiments, and the dashed-dotted line stands for the 2002 experiments.

6.2. Synoptic Variability

[37] A comparison between observed and model currents at the Fm site is provided in Figure 14, together with the corresponding temperature time series for each level. The observed currents are averaged over 3-day periods to match the subinertial model outputs. The model time series correspond to a site near the Fm mooring but further south, over a deeper isobath, in order to have data at lower levels. The deepest level represented is at 300 m instead 200 m for the observations (nominal depth). This choice was motivated by the fact that model westward flow is only noticeable at depths below 200 m (see also section 5 in Figure 6).

[38] In general, the vertical shear in the model current vector time series is lower than in the observed ones. Until mid-March, the model water column is completely homogeneous (see Figure 14) and in the first 120 m the model currents are very similar. However, after mid-March, the restratification is well reproduced by the model but the model currents are still more barotropic than the observed ones. Also, the model currents are generally more intense and persistent in direction than the observations.

[39] Since there is a low correlation between atmospheric forcing and the flow field for this slope region (as was shown before), the variability is promoted by density-driven internal variability. Since the used model does not assimilate data about the internal density fields, the model-observations comparisons may be successful in a statistical basis but the perturbations will not be in phase. However, even in a statistical point of view, the observed currents show larger variability at shorter time scales than the model. From the different model outputs (not shown), it is clear that the largest share of variability seen in the model time series is associated with meandering and with the passage over the Fm site of some coherent eddies with scales of several days (as for example the case of the mid-March reversal), whereas in the Fm observations there is a substantial amount of energy in higher-frequency movements (of the order of a few days).

[40] In summary, the model fails to reproduce two of the main characteristics observed in the synoptic Fm vector time series: the vertical shear and the significant variability at shorter time scales. The misrepresentation of the vertical shear in the model may also lead to a weaker representation of the short-scale variability, since the latter may be induced by instabilities caused by vertically sheared flow. Part of the deficient representation of high-frequency dynamics may be also attributed to the model topography (smoother that the real topography). Large vertical shears and small-scale topographic changes should promote the development of instabilities at shorter time scales leading to nonwind-driven, high-frequency dynamics.

7. Discussion and Conclusion

7.1. Inflow-Outflow Coupling and the GCC

[41] The comparative exercise between observations and the model results presented here brings further confirmation to the Gulf of Cadiz slope circulation scenario proposed before [*Kida*, 2006; *Peliz et al.*, 2007; *Kida et al.*, 2008]. The Mediterranean outflow forces a deep and broad current coastward (the Offshore Inflow current), in an opposite direction to the bottom current (the lower MO core; see Figure 2). The vertical integration of this flow produces a two dimensional cyclonic cell that matches the theoretical predictions and β plume models [*Kida*, 2006; *Kida et al.*, 2008]. The bulk of this onshore flow recirculates along with (or is entrained in) the outflow to join the Mediterranean Outflow cores. Depending on the depth level, the onshore current recirculates into the MO lower or upper core, or alternatively, at shallower levels, it feeds the inflow into the Mediterranean. It was demonstrated in Part I, and supported with additional simulations in the present study, that this current does not complement the necessary transport for the Atlantic inflow, and that this imbalance generates a secondary coastal current that dominates the upper slope/shelf break circulation all the way along the Gulf of Cadiz. An estimate of the share of the GCC to the inflow (taking a transport balance for the red box represented in Figure 2) is shown in Figure 15. The GCC approximately contributes with about 40% of the inflow. In the model, there is no clear seasonality but a strong variability at the mesoscale is apparent. Despite the differences in variability, the observations presented here and in other works [e.g., *Garcia-Lafuente et al.*, 2006; *Criado-Aldeanueva et al.*, 2006] confirm this circulation structure.

[42] *Kida* [2006] and *Kida et al.* [2008] models for the GoC slope flow show that inshore of the larger cyclonic β plume, a second anticyclonic time mean recirculation cell with transports in the order of 1 Sv is generated. This anticyclonic circulation arises from nonlinear processes in the layer above the turbulent MO, and is not necessarily associated with the inflow into the Mediterranean Sea. In our model, this second cell is constituted off the upper core MO and the GCC (Figure 2). The role of nonlinear dynamics has not been diagnosed here, but it has not been excluded either. Therefore we hypothesize that the nature of the GCC is most probably associated with the two forcings: the inflow-outflow coupling and the nonlinear effects analyzed by *Kida* [2006] and *Kida et al.* [2008].

[43] In summary, both theoretical studies (from idealized and more complex models) and the observations presented here allow us to propose a mean flow circulation scheme for the Gulf of Cadiz slope region that is dominated by two circulations cells. The cyclonic offshore cell (the β plume) is constituted of the MO lower core at depth, and of the Offshore Inflow at the upper levels. The anticyclonic inshore cell is constituted of the MO upper core and the GCC.

7.2. GCC Variability

[44] The GCC described above is driven by the MO and strait of Gibraltar exchanges, rather than by the atmospheric forcing. In fact, our results confirm that there is little covariance between winds and currents (also previously reported by *Sánchez et al.* [2006]). Since the GCC is centered at the upper slope/shelf break it would be expected that the atmospheric forcing influences or at least modulates the GCC. However, the synoptic record south of Cape St. Maria shows almost no first-order response of the currents to the wind forcing. The mooring records (Fm for example) show a highly variable flow regime which is possibly associated with either instabilities from a strongly sheared current over complex topography, or with the propagation of remotely generated perturbations. For instance, the instability in the outflow region is known to trigger waving and meandering processes in the order of 5–8 days [*Ambar et al.*, 1999; *Cherubin et al.*, 2003; *Serra et al.*, 2005; *Kida*, 2006] which are expected to propagate downstream of the main current cores. Additionally this shorter-scale variability and the vertical shear of the GCC (in weak baroclinicity) may be associated with the propagation of Coastal Trapped Waves and rectification processes that have not as yet been thoroughly investigated in the GoC. Tide have been omitted in the simulations and could be a trigger for short-scale variability.

[45] With regards to the seasonal evolution, we have seen that the mean flow is generally well reproduced by the model in the zone of the Cadiz buoy, but the winter (November–January) GCC slow down is not significant in the simulations. Since the atmospheric variability is accounted for in the model, we hypothesize that winter GCC weakening or shutoff may be associated with seasonality in the Strait of Gibraltar exchanges (which are not simulated because in the model, the inflow/outflow condition is fixed). Subinertial and seasonal variability in the exchange is still under debate. However, significant fluctuations have been reported at synoptic, seasonal and interannual scales [*Garcia Lafuente et al.*, 2002a, 2002b, 2007; *Menemenlis et al.*, 2007]. Small seasonal changes in the outflow may trigger larger changes in the surface recirculations associated with the β plume dynamics.

[46] The GCC over the slope and its non wind-driven nature may help explaining many of the SST patterns observed in the GoC such as the "Huelva front" [*Folkard et al.*, 1997; *Relvas and Barton*, 2002]. It also bears an important impact in the biogeochemical processes as it represents a steady source of upwelling onto the upper shelf. This has consequences in the seasonal evolution of the phytoplankton abundance in the slope region of active GCC, which is relatively different from other sites influenced by wind-forced upwelling [*Navarro and Ruiz*, 2006].

[47] **Acknowledgments.** This work was funded by the Fundação para a Ciência e a Tecnologia through the research contracts Clibeco (POCI/CLI/57752/2004), LobAssess (POCI/BIA-BDE/59426/2004), and AGuCa (PTDC/MAR/64902/2006). The authors thank Puertos del Estado of Spain for making available the time series at the Cadiz buoy, the Portuguese Instituto Hidrografico for Tavira wind data, and T. Reynaud for the RAFOS float processing. Very useful comments and suggestions were made by Xavier Carton, Joaquim Dias, and two anonymous reviewers.

References

Ambar, I., L. Armi, A. Bower, and T. Ferreira (1999), Some aspects of time variability of the Mediterranean Water off south Portugal, *Deep Sea Res. Part I*, *46*, 1109–1136.

Baringer, M., and J. Price (1997a), Mixing and spreading of the Mediterranean outflow, *J. Phys. Oceanogr.*, *27*(8), 1654–1677.

Baringer, M., and J. Price (1997b), Momentum and energy balance of the Mediterranean outflow, *J. Phys. Oceanogr.*, *27*(8), 1678–1692.

Borenäs, K., A. Wåhlin, I. Ambar, and N. Serra (2002), The Mediterranean outflow splitting - a comparison between theoretical models and CANIGO data, *Deep Sea Res. Part II*, *49*(19), 4195–4205.

Bower, A., B. Le Cann, T. Rossby, W. Zenk, J. Gould, K. Speer, P. Richardson, M. Prater, and H. Zhang (2002), Directly measured mid-depth circulation in the northeastern North Atlantic Ocean, *Nature*, *419*, 603–607.

Cherubin, L., N. Serra, and I. Ambar (2003), Low-frequency variability of the Mediterranean undercurrent downstream of Portimão Canyon, *J. Geophys. Res.*, *108*(C3), 3058, doi:10.1029/2001JC001229.

Criado-Aldeanueva, F., J. Garcia-Lafuente, J. M. Vargas, J. Del Rio, A. Vazquez, A. Reul, and A. Sanchez (2006), Distribution and circulation of water masses in the Gulf of Cadiz from in situ observations, *Deep Sea Res. Part II*, *53*(11–13), 1144–1160.

Folkard, A., P. Davies, A. Fiúza, and I. Ambar (1997), Remotely sensed sea surface thermal patterns in the Gulf of Cadiz and the Strait of Gibraltar: Variability, correlations, and relationships with the surface wind field, *J. Geophys. Res.*, *102*(C3), 5669–5683.

Frouin, R., A. Fiúza, I. Ambar, and T. Boyd (1990), Observations of a poleward surface current off the coasts of Portugal and Spain during winter, *J. Geophys. Res.*, *95*(C1), 679–691.

Garcia-Lafuente, J., and J. Ruiz (2007), The Gulf of Cadiz pelagic ecosystem: A review, *Prog. Oceanogr.*, *74*, 228–251.

Garcia-Lafuente, J., E. Álvarez Fanjul, J. Vargas, and A. Ratsimandresey (2002a), Subinertial variability in the flow through the Strait of Gibraltar, *J. Geophys. Res.*, *107*(C10), 3168, doi:10.1029/2001JC001104.

Garcia-Lafuente, J., J. Delgado, J. Vargas, M. Vargas, F. Plaza, and T. Sarhan (2002b), Low-frequency variability of the exchanged flows through the Strait of Gibraltar during CANIGO, *Deep Sea Res. Part II*, *49*, 4051–4067.

Garcia-Lafuente, J., J. Delgado, F. Criado-Aldeanueva, M. Bruno, J. del Rio, and J. Miguel Vargas (2006), Water mass circulation on the continental shelf of the Gulf of Cadiz, *Deep Sea Res. Part II*, *53*(11–13), 1182–1197.

Garcia-Lafuente, J., A. Sanchez Roman, G. Diaz del Rio, G. Sannino, and J. Sanchez Garrido (2007), Recent observations of seasonal variability of the Mediterranean outflow in the Strait of Gibraltar, *J. Geophys. Res.*, *112*, C10008, doi:10.1029/2007JC004238.

Huthnance, J. (1984), Slope currents and JEBAR, *J. Phys. Oceanogr.*, *14*, 795–810.

Jungclaus, J., and G. L. Mellor (2000), A three-dimensional model study of the Mediterranean outflow, *J. Mar. Syst.*, *24*, 41–66.

Kida, S. (2006), Overflows and upper ocean interaction: A mechanism for the Azores Current, Ph.D. thesis, Mass. Inst. of Technol., Cambridge, Mass. (Available at http://web.mit.edu/kida/Public/kida-Sept2006-PhDthesis.pdf)

Kida, S., J. Price, and J. Yang (2008), The upper-oceanic response to overflows: A mechanism for the Azores Current, *J. Phys. Oceanogr.*, *38*, 3–783, doi:10.1175/2007JPO3750.1.

Kundu, P. K. (1976), Ekman veering observed near the ocean bottom, *J. Phys. Oceanogr.*, *6*, 238–242.

Menemenlis, D., I. Fukumori, and T. Lee (2007), Atlantic to Mediterranean sea level difference driven by winds near Gibraltar Strait, *J. Phys. Oceanogr.*, *37*, 359–376, doi:10.1175/JPO3015.1.

Navarro, G., and J. Ruiz (2006), Spatial and temporal variability of phytoplankton in the Gulf of Cadiz through remote sensing images, *Deep Sea Res. Part II*, *53*, 1241–1260.

Papadakis, M., E. P. Chassignet, and R. W. Hallberg (2003), Numerical simulations of the Mediterranean Sea outflow: Impact of the entrainment parameterization, *Ocean Modell.*, *5*, 325–356.

Peliz, A., and A. Fiúza (1999), Temporal and spatial variability of CZCS-derived phytoplankton pigment concentrations off western Iberian Peninsula, *Int. J. Remote Sens.*, *20*(7), 1363–1403.

Peliz, A., J. Dubert, and D. Haidvogel (2003a), Subinertial response of a density driven Eastern Boundary Poleward Current to wind forcing, *J. Phys. Oceanogr.*, *33*, 1633–1650.

Peliz, A., J. Dubert, D. Haidvogel, and B. Le Cann (2003b), Generation and unstable evolution of a density-driven Eastern Poleward Current, *J. Geophys. Res.*, *108*(C8), 3268, doi:10.1029/2002JC001443.

Peliz, A., J. Dubert, A. Santos, P. Oliveira, and B. Le Cann (2005), Winter upper ocean circulation in the Western Iberian Basin—Fronts, eddies and poleward flows: An overview, *Deep Sea Res. Part I*, *52*, 621–646.

Peliz, A., J. Dubert, P. Marchesiello, and A. Teles-Machado (2007), Circulation in the Gulf of Cadiz: Model and mean flow structure, *J. Geophys. Res.*, *112*, C11015, doi:10.1029/2007JC004159.

Relvas, P., and E. Barton (2002), Mesoscale patterns in the Cape São Vicente (Iberian Peninsula) upwelling region, *J. Geophys. Res.*, *107*(C10), 3164, doi:10.1029/2000JC000456.

Sánchez, R., E. Mason, P. Relvas, A. da Silva, and A. Peliz (2006), On the inshore circulation in the northern Gulf of Cadiz, southern Portuguese shelf, *Deep Sea Res. Part II*, *53*, 1198–1218.

Serra, N., and I. Ambar (2002), Eddy generation in the Mediterranean undercurrent, *Deep Sea Res. Part II*, *49*, 4225–4243.

Serra, N., I. Ambar, and R. Käse (2005), Observations and numerical modelling of the Mediterranean outflow splitting and eddy generation, *Deep Sea Res. Part II*, *52*, 383–408.

Teles-Machado, A., A. Peliz, J. Dubert, and R. Sanchez (2007), On the onset of the Gulf of Cadiz coastal countercurrent, *Geophys. Res. Lett.*, *34*, L12601, doi:10.1029/2007GL030091.

Xu, X., E. Chassignet, J. Price, T. Ozgokmen, and H. Peters (2007), A regional modeling study of the entraining Mediterranean outflow, *J. Geophys. Res.*, *112*, C12005, doi:10.1029/2007JC004145.

J. Dubert, M. Marta-Almeida, and A. Teles-Machado, Centro de Estudos do Ambiente e do Mar, Departmento de Física, Universidade de Aveiro, P-3810-193 Aveiro, Portugal.

B. Le Cann, Laboratoire de Physique des Océans, CNRS, 6 Avenue Le Gorgeu, CS 93837, F-29238 Brest, France.

P. Marchesiello, Institut de Recherche pour le Développement, 101 Promenade Roger Laroque, B.P. A5, 98848 Noumea, New Caledonia.

A. Peliz, Instituto de Oceanografia, Universidade de Lisboa, Campo Grande, P-1749-016 Lisbon, Portugal. (ajpeliz@fc.ul.pt)

A. M. P. Santos, Instituto Nacional de Recursos Biologicos, IPIMAR, Avenida Dr. Alfredo Magalhães Ramalho s/n, P-1449-006 Lisbon, Portugal.